Spatio-angular transfer functions for fluorescence microscopes

Talon Chandler, Min Guo, Hari Shroff, Rudolf Oldenbourg, Patrick La Rivière

March 28, 2018

Abstract

We investigate how the orientation and position of fluorescent dipole emitters affects microscopic imaging using electromagnetic optics theory. Starting with the thoroughly studied spatio-angular point spread function, we introduce the spatio-angular coherent spread function, coherent transfer function, and optical transfer function as electromagnetic extensions of well-known functions in scalar optics theory. We use these concepts to show that fluorescence microscopes have a spatio-angular band limit. Finally, we study polarized light microscopes and find that polarized illumination is a type of structured illumination that extends the angular band limit.

1 Introduction

TODO

We use plain roman type for scalars, e.g., x, y, z; bold lowercase roman type for two-dimensional vectors, e.g., $\mathbf{r}$; hats for unit vectors, e.g., $\hat{\mathbf{s}}$; and bold capital roman type for matrices, e.g., $\mathbf{R}$. We use the real spherical harmonic functions

$$y_l^m(\vartheta,\varphi) = \begin{cases} \sqrt{2}K_l^m \cos(m\varphi) P_l^m(\cos\vartheta), & m > 0 \\ K_l^0 P_l^0(\cos\vartheta), & m = 0 \\ \sqrt{2}K_l^m \sin(-m\varphi) P_l^{-m}(\cos\vartheta), & m < 0 \end{cases} \tag{1}$$

where

$$K_l^m = \sqrt{\frac{(2l+1)}{4\pi}\frac{(l-|m|)!}{(l+|m|)!}}, \tag{2}$$

and $P_l^m(x)$ are the associated Legendre polynomials. The $l = 0$ and $l = 1$ spherical harmonics are given by

$$\begin{gathered} y_0^0(\vartheta,\varphi) = \sqrt{\frac{1}{4\pi}}, \\ y_1^{-1}(\vartheta,\varphi) = \sqrt{\frac{3}{4\pi}}\sin\varphi\sin\vartheta, \qquad y_1^0(\vartheta,\varphi) = \sqrt{\frac{3}{4\pi}}\cos\vartheta, \qquad y_1^1(\vartheta,\varphi) = \sqrt{\frac{3}{4\pi}}\cos\varphi\sin\vartheta. \end{gathered} \tag{3}$$

2 Spatio-angular point spread functions

Figure 1 shows a schematic of the fluorescence microscope that we are considering with a summary of our notation. We start by following Backer and Moerner [1] to find the electric field at position $\mathbf{r}_b$ in the back focal plane due to a single dipole emitter at position $\mathbf{r}_o$ oriented along $\hat{\mathbf{s}}_o$ as

$$\tilde{\mathbf{e}}_b(\mathbf{r}_b;\mathbf{r}_o,\hat{\mathbf{s}}_o) \propto \mathrm{e}^{-i(kn_o/f_o)\mathbf{r}_b\cdot\mathbf{r}_o}\sqrt{\frac{1}{\rho_b}}\begin{bmatrix} \sin^2\phi_b + \rho_b\cos^2\phi_b & \sin\phi_b\cos\phi_b(\rho_b-1) & -\frac{r_b}{f_o}\cos\phi_b \\ \sin\phi_b\cos\phi_b(\rho_b-1) & \cos^2\phi_b + \rho_b\sin^2\phi_b & -\frac{r_b}{f_o}\sin\phi_b \\ 0 & 0 & 0 \end{bmatrix}\begin{bmatrix} \cos\varphi_o\sin\vartheta_o \\ \sin\varphi_o\sin\vartheta_o \\ \cos\vartheta_o \end{bmatrix}\Pi\left(\frac{r_b}{r_b^{\max}}\right) \tag{4}$$

where we define $\rho_b \equiv \sqrt{1-\left(\frac{r_b}{f_o}\right)^2}$, and $\Pi(x)$ is a boxcar function that returns 1 when $|x| < 1$ and 0 otherwise. We can understand this expression term by term—the exponential term accounts for the phase as dipole emitter

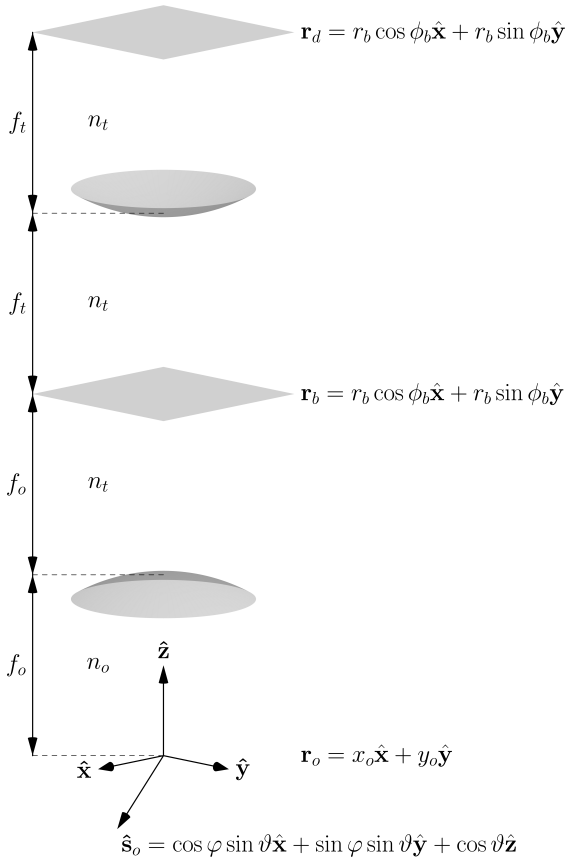

Figure 1: Simplified schematic of a single-view fluorescence microscope. The object is placed near the focal point of an aplanatic objective lens with focal length f_o in a medium with refractive index n_o. The object is parameterized by the 2D position vector $\mathbf{r}_o$ (o for object) and an orientation unit vector $\hat{\mathbf{s}}_o$. The light emitted by the fluorescent object is collected and collimated by the objective lens so that the electric fields are purely transverse in the back focal plane. Points in the back focal plane are parameterized by a 2D position vector $\mathbf{r}_b$ (b for back focal plane). Finally, the tube lens with focal length f_t refocuses the light onto a detector. Points on the detector are parameterized by a 2D position vector $\mathbf{r}_d$ (d for detector). The back focal plane and detector are in a medium with refractive index n_t. Note that this schematic is not to scale—we consider the case where $f_o \ll f_t$.

is moved in object space, the square root term conserves power before and after the objective lens, the matrix models the dipole emission process and electric field rotation caused by the objective lens, the vector is the dipole orientation unit vector, and $\Pi\left(\frac{r_b}{r_b^{\max}}\right)$ accounts for the numerical aperture of the lens with $r_b^{\max} = \frac{f_0}{n_0}\text{NA}$. We use a tilde to mark single dipole response functions—we will consider the response due to a field of dipoles in the next section.

Although we will not use the result immediately, we can write the electric field in back focal plane under the paraxial approximation. We expand Eq. 4 in a Taylor series about $r_b = 0$ and drop all second-order and higher terms to find

$$\tilde{\mathbf{e}}_b^{(p)}(\mathbf{r}_b; \mathbf{r}_o, \hat{\mathbf{s}}_o) \propto \mathrm{e}^{-i(kn_o/f_o)\mathbf{r}_b \cdot \mathbf{r}_o} \begin{bmatrix} 1 & 0 & -\frac{r_b}{f_o}\cos\phi_b \\ 0 & 1 & -\frac{r_b}{f_o}\sin\phi_b \\ 0 & 0 & 0 \end{bmatrix} \begin{bmatrix} \cos\varphi_o \sin\vartheta_o \\ \sin\varphi_o \sin\vartheta_o \\ \cos\vartheta_o \end{bmatrix} \Pi\left(\frac{r_b}{r_b^{\max}}\right) \tag{5}$$

We will continue to use a superscript (p) to mark terms that have used the paraxial approximation.

If the tube lens is weakly focusing ($f_o \ll f_t$) then we can find the electric field in the detector plane by

taking the Fourier transform of the electric field in the back focal plane

$$\tilde{\mathbf{e}}_d(\mathbf{r}_d;\mathbf{r}_o,\hat{\mathbf{s}}_o) \propto \int_{\mathbb{R}^2} d\mathbf{r}_b\, \tilde{\mathbf{e}}_b(\mathbf{r}_b;\mathbf{r}_o,\hat{\mathbf{s}}_o)\mathrm{e}^{-i(kn_t/f_t)\mathbf{r}_b\cdot\mathbf{r}_d}. \tag{6}$$

By isolating the phase term in Eq. 4 with $\tilde{\mathbf{e}}_b(\mathbf{r}_b;\mathbf{r}_o,\hat{\mathbf{s}}_o) \equiv \mathrm{e}^{-i(kn_o/f_o)\mathbf{r}_b\cdot\mathbf{r}_o}\underline{\tilde{\mathbf{e}}}_b(\mathbf{r}_b;\hat{\mathbf{s}}_o)$, and plugging into Eq. 6 we find that

$$\tilde{\mathbf{e}}_d(\mathbf{r}_d - M\mathbf{r}_o,\hat{\mathbf{s}}_o) \propto \int_{\mathbb{R}^2} d\mathbf{r}_b\, \underline{\tilde{\mathbf{e}}}_b(\mathbf{r}_b;\hat{\mathbf{s}}_o)\mathrm{e}^{-i(kn_t/f_t)\,\mathbf{r}_b\cdot[\mathbf{r}_d - M\mathbf{r}_o]}. \tag{7}$$

where $M = -\frac{n_o}{n_t}\frac{f_t}{f_o}$ is the transverse magnification. By writing the electric field in the detector plane in terms of $\mathbf{r}_d - M\mathbf{r}_o$, we have established that the electric field in the detector plane is *transverse shift-invariant*—a transverse shift of the object creates a magnified transverse shift of the image. We define coordinates on the detector centered on the image of the object $\mathbf{r}'_d \equiv \mathbf{r}_d - M\mathbf{r}_o = r'_d\cos\phi'_d\hat{\mathbf{x}} + r'_d\sin\phi'_d\hat{\mathbf{y}}$, then we follow Novotny [2] by writing the integrals in polar coordinates, evaluating the azimuthal integrals, and writing the result concisely in terms of three radial integrals

$$\tilde{\mathbf{e}}_d(\mathbf{r}'_d,\hat{\mathbf{s}}_o) \propto \begin{bmatrix} A(r'_d) + C(r'_d)\cos(2\phi'_d) & C(r'_d)\sin(2\phi'_d) & 2iB(r'_d)\cos\phi'_d \\ C(r'_d)\sin(2\phi'_d) & A(r'_d) - C(r'_d)\cos(2\phi'_d) & 2iB(r'_d)\sin\phi'_d \\ 0 & 0 & 0 \end{bmatrix} \begin{bmatrix} \cos\varphi_o\sin\vartheta_o \\ \sin\varphi_o\sin\vartheta_o \\ \cos\vartheta_o \end{bmatrix} \tag{8}$$

where $A(r'_d), B(r'_d)$, and $C(r'_d)$ are

$$A(r'_d) = \int_0^{\theta_{\max}} d\theta\ \sqrt{\cos\theta}\sin\theta(1+\cos\theta)J_0(k_b r'_d\sin\theta f_o/f_t), \tag{9}$$

$$B(r'_d) = \int_0^{\theta_{\max}} d\theta\ \sqrt{\cos\theta}\sin^2\theta J_1(k_b r'_d\sin\theta f_o/f_t), \tag{10}$$

$$C(r'_d) = \int_0^{\theta_{\max}} d\theta\ \sqrt{\cos\theta}\sin\theta(1-\cos\theta)J_2(k_b r'_d\sin\theta f_o/f_t). \tag{11}$$

We can identify Eq. 8 as the vector-valued *coherent spread function* (CSF) of the microscope. The scalar-valued CSF—sometimes called the amplitude transfer function—is only applicable to cases where electromagnetic optics plays no role in the microscope—not true for samples that contain dipole emitters.

To build our intuition about the CSF, we will rewrite the matrix multiplication in Eq. 8 in terms of the spherical harmonics. Notice that the $l = 1$ spherical harmonics are the Cartesian components of the unit dipole axis (see Eq. 3), so the CSF becomes

$$\tilde{\mathbf{e}}_d(\mathbf{r}'_d,\hat{\mathbf{s}}_o) \propto \begin{bmatrix} [A(r'_d) + C(r'_d)\cos(2\phi'_d)]y_1^1(\hat{\mathbf{s}}_o) + C(r'_d)\sin(2\phi'_d)y_1^{-1}(\hat{\mathbf{s}}_o) + 2iB(r'_d)\cos\phi'_d y_1^0(\hat{\mathbf{s}}_o) \\ C(r'_d)\sin(2\phi'_d)y_1^1(\hat{\mathbf{s}}_o) + [A(r'_d) - C(r'_d)\cos(2\phi'_d)]y_1^{-1}(\hat{\mathbf{s}}_o) + 2iB(r'_d)\sin\phi'_d y_1^0(\hat{\mathbf{s}}_o) \\ 0 \end{bmatrix}. \tag{12}$$

By applying the paraxial approximation ($\sin\theta \approx \theta$ and $\cos\theta \approx 1$), the integrals $A(r'_d), B(r'_d)$ and $C(r'_d)$ can be evaluated in terms of Bessel functions. We can evaluate $A(r'_d)$ and $B(r'_d)$ with the help of $\int_0^z dx\ xJ_0(ax) = zJ_1(az)/a$ and $\int_0^z dx\ x^2J_1(ax) = z^2J_2(az)/a$, respectively, and $C(r'_d) = 0$ because $J_2(x)$ is zero to first order. In this case, the CSF simplifies to

$$\tilde{\mathbf{e}}_d^{(p)}(\mathbf{r}'_d,\hat{\mathbf{s}}_o) \propto \begin{bmatrix} A^{(p)}(r'_d)y_1^1(\hat{\mathbf{s}}_o) + 2iB^{(p)}(r'_d)\cos\phi'_d y_1^0(\hat{\mathbf{s}}_o) \\ A^{(p)}(r'_d)y_1^{-1}(\hat{\mathbf{s}}_o) + 2iB^{(p)}(r'_d)\sin\phi'_d y_1^0(\hat{\mathbf{s}}_o) \\ 0 \end{bmatrix} \tag{13}$$

where the integrals evaluate to

$$A^{(p)}(r'_d) = \frac{J_1(2\pi a r'_d)}{\pi a r'_d}, \qquad B^{(p)}(r'_d) = \frac{\mathrm{NA}}{n_o}\left[\frac{J_2(2\pi a r'_d)}{\pi a r'_d}\right], \tag{14}$$

and we have substituted

$$a \equiv \frac{\mathrm{NA}}{M\lambda}, \qquad \mathrm{NA} \equiv n_o \sin\theta_{\max}. \tag{15}$$

Under the paraxial approximation the electric fields on the detector created by a single dipole are composed of two parts, a parallel part and a radial part. The coefficients of the y_1^0 spherical harmonic in Eq. 13 create the radial part of the field—the z component of the dipole generates a radial field on the detector with respect to the image point. The coefficients of the y_1^1 and y_1^{-1} spherical harmonics create a parallel field in the detector plane parallel to the x and y components of the dipole. As the NA increases and the paraxial approximation no longer applies, we begin to see coupling between the $x(y)$ component of the dipole with the $y(x)$ transverse field.

We can find the intensity in the detector plane due to a single dipole by taking the modulus squared of the CSF

$$h(\mathbf{r}'_d, \hat{\mathbf{s}}_o) = \left|\tilde{\mathbf{e}}_d(\mathbf{r}'_d, \hat{\mathbf{s}}_o)\right|^2. \tag{16}$$

For convenience we keep the CSF written in terms of the spherical harmonics and use a table of spherical harmonic products (see Appendix A) to calculate the intensity in the detector plane as

$$\begin{aligned} h(\mathbf{r}'_d, \hat{\mathbf{s}}_o) \propto{}& \left(A^2(r'_d) + 2B^2(r'_d) + C^2(r'_d)\right) y_0^0(\hat{\mathbf{s}}_o) - \frac{2\sqrt{15}}{5} A(r'_d)C(r'_d)\sin(2\phi'_d) y_2^{-2}(\hat{\mathbf{s}}_o) \\ &+ \frac{1}{\sqrt{5}}\left(-A^2(r'_d) + 4B^2(r'_d) - C^2(r'_d)\right) y_2^0(\hat{\mathbf{s}}_o) + \frac{2\sqrt{15}}{5} A(r'_d)C(r'_d)\cos(2\phi'_d) y_2^2(\hat{\mathbf{s}}_o). \end{aligned} \tag{17}$$

We can identify Eq. 17 as the spatio-angular *point spread function* (PSF) of the microscope. Writing the spatio-angular PSF in terms of spherical harmonic functions has two advantages. First, it allows us to express the spatio-angular PSF very concisely. Instead of considering the point spread function for every possible dipole orientation, we only need to consider four spatio-angular PSFs—one for each spherical harmonic. Second, the spherical harmonic functions form an orthonormal basis for functions on the sphere—a convenient fact that we will use later.

It is useful to compare Eq. 17 to Backer and Moerner's approach [1]. They expand the spatio-angular PSF in terms of six second moments of the fluorophore distribution $\{s_x^2, s_y^2, s_z^2, s_x s_y, s_x s_z, s_y s_z\}$. This approach is very useful—only six precomputed spatio-angular PSFs are required to represent an arbitrary spatio-angular PSF. Instead of expanding in terms of six second moments, we expand onto just four spherical harmonics which, unlike the second moments, are orthonormal functions. In the next section we will use the orthonormality of the spherical harmonics to derive spatio-angular transfer functions for fluorescence microscopes.

The spatio-angular PSF under the paraxial approximation is given by

$$h^{(p)}(\mathbf{r}'_d, \hat{\mathbf{s}}_o) \propto \left({A^{(p)}}^2(r'_d) + 2{B^{(p)}}^2(r'_d)\right) y_0^0(\hat{\mathbf{s}}_o) + \frac{1}{\sqrt{5}}\left(-{A^{(p)}}^2(r'_d) + 4{B^{(p)}}^2(r'_d)\right) y_2^0(\hat{\mathbf{s}}_o). \tag{18}$$

First, consider the coefficient on the y_0^0 spherical harmonic in Eq. 18. This coefficient is the point spread function for an angularly uniform distribution of fluorophores. The first term of the coefficient ${A^{(p)}}^2(r'_d)$ is the familiar Airy disk that arises from the contribution of dipoles oriented in the transverse plane, while the second term ${B^{(p)}}^2(r'_d)$ is a smaller factor that arises from dipoles oriented outside of the transverse plane. This leads

to an interesting conclusion—a uniform distribution of dipoles has a point spread function that is slightly wider than an Airy disk even in the paraxial approximation. The Airy disk is usually derived using paraxial scalar optics while here we have used paraxial electromagnetic optics. Therefore, we can consider the second term to be an electromagnetic correction to the Airy disk. We will quantify this difference in the next section.

Next, consider the coefficient on the y_2^0 spherical harmonic in Eq. 18. This coefficient is the spatial PSF for a distribution of fluorophores proportional to $3\cos^2\vartheta_o - 1$. Counterintuitively, this fluorophore distribution cannot exist because it would require a negative number of fluorophores along some orientations; but if this distribution could exist, then this coefficient would be its spatial PSF. Considering negative distributions of fluorophores in our calculations should not be cause for concern. The spherical harmonics span the space of functions on the sphere, so any positive fluorophore distribution can be represented by the spherical harmonics and we never need to consider negative fluorophores.

Finally, consider all of the spherical harmonics that have a zero coefficient. These spherical harmonics span the angular null space of our measurement system—fluorophore distributions that lie in the null space do not affect the measured intensities. Under the paraxial approximation all of the non-zero coefficients are rotationally symmetric ($m = 0$) spherical harmonics which means that the transverse orientation of the dipoles does not affect the PSF. In the high NA case this is no longer true—two $m = 2$ spherical harmonics have non-zero coefficients and the transverse orientation of dipoles does affect the PSF.

3 Spatio-angular transfer functions

Consider a thin object that consists of fluorescent dipoles in arbitrary positions and orientations. We can represent the entire object using a function $\boldsymbol{\mu}(\mathbf{r}_o, \hat{\mathbf{s}}_o)$ that returns a complex-valued vector for each position $\mathbf{r}_o$ and direction $\hat{\mathbf{s}}_o$. The magnitude of the complex-valued vector is the magnitude of the dipole moment and the elements of the vector give the orientation and phase of the radiating dipole moment. Because $\boldsymbol{\mu}(\mathbf{r}_o, \hat{\mathbf{s}}_o)$ includes the relative phases of different points and orientations in the object, $\boldsymbol{\mu}(\mathbf{r}_o, \hat{\mathbf{s}}_o)$ can represent coupled dipoles that are emitting partially or completely coherently.

We can find the electric field on the detector created by this object by multiplying $\boldsymbol{\mu}(\mathbf{r}_o, \hat{\mathbf{s}}_o)$ with the CSF then integrating over all positions and orientations in the object

$$\mathbf{e}_d(\mathbf{r}_d) = \int_{\mathbb{S}^2} d\hat{\mathbf{s}}_o \int_{\mathbb{R}^2} d\mathbf{r}_o \; \tilde{\mathbf{e}}_d(\mathbf{r}_d - M\mathbf{r}_o, \hat{\mathbf{s}}_o)\boldsymbol{\mu}(\mathbf{r}_o, \hat{\mathbf{s}}_o). \tag{19}$$

Note that these integrals represent a vector sum—the coherence of the electric fields radiated by the object can cause cancellations of the fields created on the detector.

We can simplify this expression by expanding the CSF in terms of spatio-angular harmonics

$$\tilde{\mathbf{e}}_d(\mathbf{r}_d - M\mathbf{r}_o, \hat{\mathbf{s}}_o) = \sum_{l=0}^{\infty} \sum_{m=-l}^{l} \int_{\mathbb{R}^2} d\boldsymbol{\nu}\, \mathbf{E}_l^m(\boldsymbol{\nu}) y_l^m(\hat{\mathbf{s}}_o)\, \mathrm{e}^{i2\pi(\mathbf{r}_d - M\mathbf{r}_o)\cdot\boldsymbol{\nu}}, \tag{20}$$

where $\mathbf{E}_l^m(\boldsymbol{\nu})$ is the spatio-angular spectrum of the CSF given by

$$\mathbf{E}_l^m(\boldsymbol{\nu}) \equiv \int_{\mathbb{S}^2} d\hat{\mathbf{s}}_o \int_{\mathbb{R}^2} d\mathbf{r}_o\, \tilde{\mathbf{e}}_d(\mathbf{r}_d - M\mathbf{r}_o, \hat{\mathbf{s}}_o) y_l^m(\hat{\mathbf{s}}_o)\, \mathrm{e}^{-i2\pi(\mathbf{r}_d - M\mathbf{r}_o)\cdot\boldsymbol{\nu}}. \tag{21}$$

We can change variables to make this expression easier to evaluate

$$\mathbf{E}_l^m(\boldsymbol{\nu}) \propto \int_{\mathbb{S}^2} d\hat{\mathbf{s}}_o \int_{\mathbb{R}^2} d\mathbf{r}_o\, \tilde{\mathbf{e}}_d(\mathbf{r}'_d, \hat{\mathbf{s}}_o) y_l^m(\hat{\mathbf{s}}_o)\, \mathrm{e}^{-i2\pi\mathbf{r}'_d\cdot\boldsymbol{\nu}}. \tag{22}$$

By plugging Eq. 20 into Eq. 19 we find that

$$\mathbf{e}_d(\mathbf{r}_d) = \int_{\mathbb{S}^2} d\hat{\mathbf{s}}_o \int_{\mathbb{R}^2} d\mathbf{r}_o \left[\sum_{l=0}^{\infty} \sum_{m=-l}^{l} \int_{\mathbb{R}^2} d\boldsymbol{\nu}\, \mathbf{E}_l^m(\boldsymbol{\nu}) y_l^m(\hat{\mathbf{s}}_o)\, \mathrm{e}^{i2\pi(\mathbf{r}_d - M\mathbf{r}_o)\cdot\boldsymbol{\nu}} \right] \boldsymbol{\mu}(\mathbf{r}_o, \hat{\mathbf{s}}_o). \tag{23}$$

We can rearrange this equation into the following form

$$\mathbf{e}_d(\mathbf{r}_d) = \sum_{l=0}^{\infty} \sum_{m=-l}^{l} \int_{\mathbb{R}^2} d\boldsymbol{\nu}\, \mathbf{E}_l^m(\boldsymbol{\nu}) \left[\int_{\mathbb{S}^2} d\hat{\mathbf{s}}_o \int_{\mathbb{R}^2} d\mathbf{r}_o\, \boldsymbol{\mu}(\mathbf{r}_o, \hat{\mathbf{s}}_o) y_l^m(\hat{\mathbf{s}}_o)\, \mathrm{e}^{-i2\pi M \mathbf{r}_o \cdot \boldsymbol{\nu}} \right] \mathrm{e}^{i2\pi \mathbf{r}_d \cdot \boldsymbol{\nu}}. \tag{24}$$

We recognize the term in square brackets as the spatio-angular spectrum of the object, so we define

$$\mathbf{M}_l^m(\boldsymbol{\nu}) \equiv \int_{\mathbb{S}^2} d\hat{\mathbf{s}}_o \int_{\mathbb{R}^2} d\mathbf{r}_o\, \boldsymbol{\mu}(\mathbf{r}_o, \hat{\mathbf{s}}_o) y_l^m(\hat{\mathbf{s}}_o)\, \mathrm{e}^{-i2\pi M \mathbf{r}_o \cdot \boldsymbol{\nu}}. \tag{25}$$

and write the electric field on the detector as

$$\mathbf{e}_d(\mathbf{r}_d) = \sum_{l=0}^{\infty} \sum_{m=-l}^{l} \int_{\mathbb{R}^2} d\boldsymbol{\nu}\, \mathbf{E}_l^m(\boldsymbol{\nu}) \mathbf{M}_l^m(\nu) \mathrm{e}^{i2\pi \mathbf{r}_d \cdot \boldsymbol{\nu}}. \tag{26}$$

Eq. 35 shows that the electric field on the detector can be found by resolving the object into its spatio-angular components $\mathbf{M}_l^m(\boldsymbol{\nu})$, weighting each component by $\mathbf{E}_l^m(\boldsymbol{\nu})$, then summing over all spatio-angular components. Therefore, we identify $\mathbf{E}_l^m(\boldsymbol{\nu})$ as the spatio-angular *coherent transfer function* (CTF).

In Appendix B we calculate the paraxial CTF for a single-view fluorescence microscope as

$$\mathbf{E}_l^{m(p)}(\boldsymbol{\nu}) = \begin{bmatrix} \delta(l-1, m-1) + \frac{2}{a} \frac{\mathrm{NA}}{n_o} \nu \cos\phi_\nu \delta(l-1, m) \\ \delta(l-1, m+1) + \frac{2}{a} \frac{\mathrm{NA}}{n_o} \nu \sin\phi_\nu \delta(l-1, m) \\ 0 \end{bmatrix} \Pi\left(\frac{\nu}{a}\right). \tag{27}$$

The CTF shows that single-view coherent microscopes have a spatial band limit at $\nu = a$ and an $l = 1$ angular pass band. It is useful to compare the paraxial CTF in Eq. 27 to the paraxial electric field in the back focal plane in Eq. 5. The CTF is just a rescaled version of the electric field in the back focal plane, and this leads to an extremely valuable interpretation. The CTF of a single-view fluorescence microscope is constrained to the three members of the $l = 1$ band the value of the CTF for each m is a rescaled version of the electric field due to a single dipole oriented along one of the Cartesian axes.

At the risk of being too explicit, the $m = 1$ CTF is a rescaled version of the electric field due to a dipole oriented along the x axis, the $m = -1$ CTF is a rescaled version of the electric field due to a dipole oriented along the y axis, and the $m = 0$ CTF is a rescaled version of the electric field due to a dipole oriented along the z axis. Therefore, we can reason about the CTF by thinking about the electric field that single x-, y-, and z-oriented dipoles create in the back focal plane.

With this interpretation in mind, the form of the CTF is not surprising. Under the paraxial approximation x- and y-oriented dipoles uniformly fill the back focal plane with an electric field parallel to the dipole axis. A z-oriented dipole creates a radial electric field with linearly increasing amplitude towards the edges of the back focal plane.

The spatial band limit can be increased by increasing the NA of the microscope, so what parameter sets the angular band limit? The angular band limit in the current microscope is set by the dipole emission process—only $l = 1$ terms show up in the CTF for dipole emitters. Adding polarizing filters to the microscope will not extend the band limit of the microscope because filters only block electric fields. However, polarized illumination can be used to extend the band limit. The excitation process is completely incoherent with the emission process, so the spatio-angular transfer functions of the two processes will multiply. We can use the multiplication rules in Appendix A to find the band limit of the new microscope that uses selective excitation.

Next we find the intensity on the detector plane $g(\mathbf{r}_d)$ by taking the modulus squared of the electric field. Using Eq. 19 we find that

$$g(\mathbf{r}_d) = |\mathbf{e}_d(\mathbf{r}_d)|^2 = \left| \int_{\mathbb{S}^2} d\hat{\mathbf{s}}_o \int_{\mathbb{R}^2} d\mathbf{r}_o\, \tilde{\mathbf{e}}_d(\mathbf{r}_d - M\mathbf{r}_o, \hat{\mathbf{s}}_o) \boldsymbol{\mu}(\mathbf{r}_o, \hat{\mathbf{s}}_o) \right|^2. \tag{28}$$

If the dipoles emit incoherently—a fair assumption for fluorescent emitters that are not within homo-FRET distance—then we can take the modulus squared of the object and CSF independently which gives

$$g(\mathbf{r}_d) = \int_{\mathbb{S}^2} d\hat{\mathbf{s}}_o \int_{\mathbb{R}^2} d\mathbf{r}_o \; \left|\tilde{\mathbf{e}}_d(\mathbf{r}_d - M\mathbf{r}_o, \hat{\mathbf{s}}_o)\right|^2 \left|\boldsymbol{\mu}(\mathbf{r}_o, \hat{\mathbf{s}}_o)\right|^2. \tag{29}$$

We recognize that $\left|\tilde{\mathbf{e}}_d(\mathbf{r}_d - M\mathbf{r}_o, \hat{\mathbf{s}}_o)\right|^2$ is the PSF of the microscope $h(\mathbf{r}_d - M\mathbf{r}_o, \hat{\mathbf{s}}_o)$, and we introduce a new function $f(\mathbf{r}_o, \hat{\mathbf{s}}_o) \equiv \left|\boldsymbol{\mu}(\mathbf{r}_o, \hat{\mathbf{s}}_o)\right|^2$ to represent the object

$$g(\mathbf{r}_d) = \int_{\mathbb{S}^2} d\hat{\mathbf{s}}_o \int_{\mathbb{R}^2} d\mathbf{r}_o \; h(\mathbf{r}_d - M\mathbf{r}_o, \hat{\mathbf{s}}_o) f(\mathbf{r}_o, \hat{\mathbf{s}}_o). \tag{30}$$

We can interpret $f(\mathbf{r}_o, \hat{\mathbf{s}}_o)$ as the spatio-angular density of dipoles—it is a function that is proportional to the number of fluorophores at position $\mathbf{r}_o$ oriented in direction $\hat{\mathbf{s}}_o$ per unit volume per unit solid angle. Notice that h and f are scalar functions—we removed all phase information when we took the modulus squared.

We can follow our previous work with the electric field and simplify Eq. 30 by expanding the PSF in terms of spatio-angular harmonics

$$h(\mathbf{r}_d - M\mathbf{r}_o, \hat{\mathbf{s}}_o) = \sum_{l=0}^{\infty} \sum_{m=-l}^{l} \int_{\mathbb{R}^2} d\boldsymbol{\nu} \, H_l^m(\boldsymbol{\nu}) y_l^m(\hat{\mathbf{s}}_o) \, \mathrm{e}^{i2\pi(\mathbf{r}_d - M\mathbf{r}_o)\cdot\boldsymbol{\nu}}, \tag{31}$$

where $H_l^m(\boldsymbol{\nu})$ is the spatio-angular spectrum of the PSF given by

$$H_l^m(\boldsymbol{\nu}) \equiv \int_{\mathbb{S}^2} d\hat{\mathbf{s}}_o \int_{\mathbb{R}^2} d\mathbf{r}_o \, h(\mathbf{r}_d - M\mathbf{r}_o, \hat{\mathbf{s}}_o) y_l^m(\hat{\mathbf{s}}_o) \, \mathrm{e}^{-i2\pi(\mathbf{r}_d - M\mathbf{r}_o)\cdot\boldsymbol{\nu}}. \tag{32}$$

We can change variables to make this expression easier to evaluate

$$H_l^m(\boldsymbol{\nu}) \propto \int_{\mathbb{S}^2} d\hat{\mathbf{s}}_o \int_{\mathbb{R}^2} d\mathbf{r}'_d \, h(\mathbf{r}'_d, \hat{\mathbf{s}}_o) y_l^m(\hat{\mathbf{s}}_o) \, \mathrm{e}^{-i2\pi\mathbf{r}'_d\cdot\boldsymbol{\nu}}. \tag{33}$$

By plugging Eq. 31 into Eq. 30 we find that

$$g(\mathbf{r}_d) = \int_{\mathbb{S}^2} d\hat{\mathbf{s}}_o \int_{\mathbb{R}^2} d\mathbf{r}_o \left[\sum_{l=0}^{\infty} \sum_{m=-l}^{l} \int_{\mathbb{R}^2} d\boldsymbol{\nu} \, H_l^m(\boldsymbol{\nu}) y_l^m(\hat{\mathbf{s}}_o) \, \mathrm{e}^{i2\pi(\mathbf{r}_d - M\mathbf{r}_o)\cdot\boldsymbol{\nu}} \right] f(\mathbf{r}_o, \hat{\mathbf{s}}_o). \tag{34}$$

We can rearrange this equation into the following form

$$g(\mathbf{r}_d) = \sum_{l=0}^{\infty} \sum_{m=-l}^{l} \int_{\mathbb{R}^2} d\boldsymbol{\nu} \, H_l^m(\boldsymbol{\nu}) \left[\int_{\mathbb{S}^2} d\hat{\mathbf{s}}_o \int_{\mathbb{R}^2} d\mathbf{r}_o \, f(\mathbf{r}_o, \hat{\mathbf{s}}_o) y_l^m(\hat{\mathbf{s}}_o) \, \mathrm{e}^{-i2\pi M\mathbf{r}_o\cdot\boldsymbol{\nu}} \right] \mathrm{e}^{i2\pi\mathbf{r}_d\cdot\boldsymbol{\nu}}. \tag{35}$$

We recognize the term in square brackets as the spatio-angular spectrum of the object, so we define

$$F_l^m(\boldsymbol{\nu}) \equiv \int_{\mathbb{S}^2} d\hat{\mathbf{s}}_o \int_{\mathbb{R}^2} d\mathbf{r}_o \, f(\mathbf{r}_o, \hat{\mathbf{s}}_o) y_l^m(\hat{\mathbf{s}}_o) \, \mathrm{e}^{-i2\pi M\mathbf{r}_o\cdot\boldsymbol{\nu}}. \tag{36}$$

and write the intensity on the detector as

$$g(\mathbf{r}_d) = \sum_{l=0}^{\infty} \sum_{m=-l}^{l} \int_{\mathbb{R}^2} d\boldsymbol{\nu} \, H_l^m(\boldsymbol{\nu}) F_l^m(\nu) \mathrm{e}^{i2\pi\mathbf{r}_d\cdot\boldsymbol{\nu}}. \tag{37}$$

Eq. 37 shows that the intensity on the detector can be found by resolving the object into its spatio-angular component $F_l^m(\nu_o)$, weighting each component by $H_l^m(\nu_o)$, then summing over all spatio-angular components. Therefore, we identify $H_l^m(\nu_o)$ as the spatio-angular *optical transfer function* (OTF). Notice that the CSF and CTF are vector-valued functions, while the PSF and OTF are scalar-valued functions.

In Appendix C we calculate the paraxial OTF for a single-view fluorescence microscope as

The spatio-angular OTF measures the ability of the microscope to pass spatio-angular harmonics—instead of the usual spatial harmonics $\mathrm{e}^{i2\pi\mathbf{r}_o\cdot\boldsymbol{\nu}}$ we now need consider the spatio-angular harmonics $y_l^m(\hat{\mathbf{s}}_o)\,\mathrm{e}^{i2\pi\mathbf{r}_o\cdot\boldsymbol{\nu}}$. Eq. **??** can be interpreted as the spatio-angular Fourier transform of the spatio-angular PSF.

We can plug Eq. 17 into **??** and use the orthonormality relation for spherical harmonics $\int_{\mathbb{S}^2} d\hat{\mathbf{s}}_o y_{l_0}^{m_0}(\hat{\mathbf{s}}_o) y_{l_1}^{m_1}(\hat{\mathbf{s}}_o) = \delta(l_0 - l_1, m_0 - m_1)$ to find that

$$\begin{aligned} H_l^m(\boldsymbol{\nu}) \propto \int_{\mathbb{R}^3} d\mathbf{r}_o \Bigg[& \left(I_0^2 + 2I_1^2 + I_2^2\right)\delta(l,m) - \frac{2\sqrt{15}}{5} I_0 I_2 \sin(2\phi_d)\,\delta(l-2,m+2) \\ & + \frac{1}{\sqrt{5}}\left(-I_0^2 + 4I_1^2 - I_2^2\right)\delta(l-2,m) + \frac{2\sqrt{15}}{5} I_0 I_2 \cos(2\phi_d)\,\delta(l-2,m-2)\Bigg] \mathrm{e}^{i2\pi\mathbf{r}_o\cdot\boldsymbol{\nu}}. \end{aligned} \tag{38}$$

We can see that the microscope has an angular band limit—the microscope only passes intensity contributions for fluorophore distributions in the $l = 0$ and $l = 2$ bands.

Once again, we constrain the object to the focal plane and apply the paraxial approximation to find that

$$H_l^{m(p)}(\nu^x, \nu^y) \propto \int_{\mathbb{R}^2} d\mathbf{r}_o \left[\left(I_0^{(p)^2} + 2I_1^{(p)^2}\right)\delta(l,m) + \frac{1}{\sqrt{5}}\left(-I_0^{(p)^2} + 4I_1^{(p)^2}\right)\delta(l-2,m)\right] \mathrm{e}^{i2\pi(\nu^x x_o + \nu^y y_o)} \tag{39}$$

The integral in Eqs. 39 cannot be solved directly. We could proceed numerically like [1], but instead we use the Wiener-Khinchin theorem to simplify the integral [3, 4]. We complete the calculation in Appendix C and find that The final paraxial OTF for a single-view fluorescence microscope is given by

$$H_l^m(\boldsymbol{\nu}) \tag{40}$$

TODO: The auto-correlation calculation is in progress. I should be able to find an analytic formula for the OTF, but for now I am plotting it numerically in Figure 3.

TODO: Plot PSFs and OTFs numerically without the paraxial approximation.

TODO: Consider detection polarizers.

TODO: Consider illumination polarizers.

4 Conclusions

TODO

References

[1] Adam S. Backer and W. E. Moerner. Extending single-molecule microscopy using optical Fourier processing. *J. Phys. Chem. B*, 118(28):8313–8329, 2014.

[2] Lukas Novotny and Bert Hecht. *Principles of Nano-Optics*. Cambridge University Press, 2006.

[3] J.W. Goodman. *Introduction to Fourier Optics*. McGraw-Hill, 2nd edition, 1996.

[4] A. Papoulis and S. U. Pillai. *Probability, Random Variables, and Stochastic Processes*. McGraw-Hill Higher Education, 4 edition, 2002.

[5] J. Mertz. *Introduction to Optical Microscopy*. W. H. Freeman, 2009.

[6] A. Poularikas. *Handbook of Formulas and Tables for Signal Processing*. Electrical Engineering Handbook. CRC-Press, 1998.

[7] `http://mathworld.wolfram.com/Wiener-KhinchinTheorem.html`.

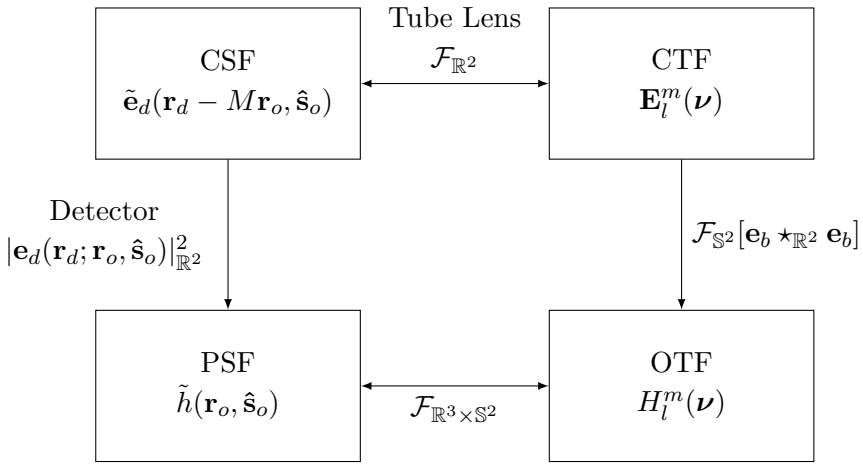

Figure 2: Summary of relationships between the CSF, CTF, PSF, and OTF where $\mathcal{F}_D$, $|\cdot|_D$, and $\star_D$ denote the Fourier transform, norm, and autocorrelation over the set D, respectively. See [3] and [5] for analogous diagrams under scalar optics approximations.

A Products of real spherical harmonics

The six products of $l = 1$ spherical harmonics are

$$y_1^{-1} y_1^{-1} \sqrt{\pi} = \frac{1}{2} y_0^0 - \frac{\sqrt{5}}{10} y_2^0 - \frac{\sqrt{15}}{10} y_2^2, \tag{41}$$

$$y_1^{-1} y_1^0 \sqrt{\pi} = \frac{\sqrt{15}}{10} y_2^{-1}, \tag{42}$$

$$y_1^{-1} y_1^1 \sqrt{\pi} = -\frac{\sqrt{15}}{10} y_2^{-2}, \tag{43}$$

$$y_1^0 y_1^0 \sqrt{\pi} = \frac{1}{2} y_0^0 + \frac{\sqrt{5}}{5} y_2^0, \tag{44}$$

$$y_1^0 y_1^1 \sqrt{\pi} = \frac{\sqrt{15}}{10} y_2^1, \tag{45}$$

$$y_1^1 y_1^1 \sqrt{\pi} = \frac{1}{2} y_0^0 - \frac{\sqrt{5}}{10} y_2^0 + \frac{\sqrt{15}}{10} y_2^2. \tag{46}$$

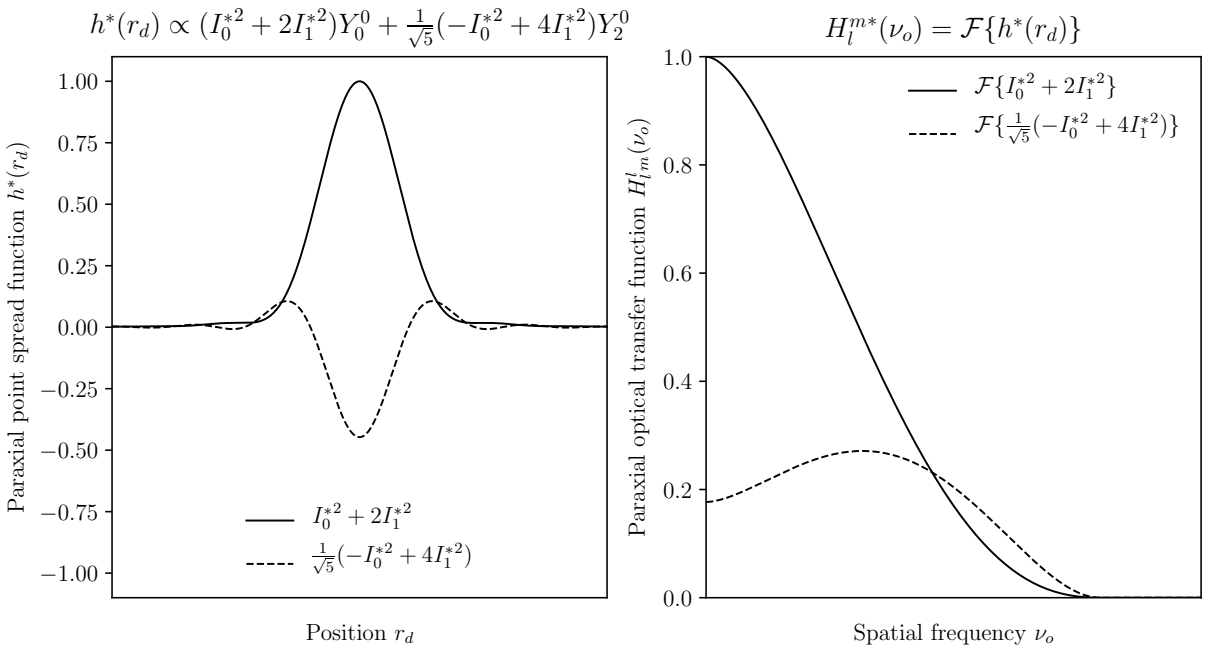

Figure 3: In progress. **Left:** Paraxial spatio-angular point spread function for a single-view fluorescence microscope with NA=0.8. The solid line is the PSF for y_0^0 distributions and the dashed line is the PSF for y_2^0 distributions. y_2^0 includes "negative" fluorophores, so it gives rise to a negative PSF. **Right:** Numerical paraxial spatio-angular optical transfer function for the same microscope. The y_0^0 term has a spatial low-pass response while the y_2^0 term has a spatial high-pass response. The relative sizes of the two terms is set by the NA—increasing the NA increases the relative size of the y_0^2 term. Vertical scaling is correct—horizontal scaling is in progress. The cutoff frequency is proportional to NA and is the same for both spherical harmonic terms.

The fifteen products of $l = 2$ spherical harmonics are

$$y_2^{-2}y_2^{-2}\sqrt{\pi} = \frac{1}{2}y_0^0 - \frac{\sqrt{5}}{7}y_2^0 + \frac{1}{14}y_4^0 - \frac{\sqrt{35}}{14}y_4^4 \tag{47}$$

$$y_2^{-2}y_2^{-1}\sqrt{\pi} = -\frac{\sqrt{15}}{14}y_2^1 + \frac{\sqrt{10}}{28}y_4^1 + \frac{\sqrt{70}}{28}y_4^3 \tag{48}$$

$$y_2^{-2}y_2^{0}\sqrt{\pi} = -\frac{\sqrt{5}}{7}y_2^{-2} + \frac{\sqrt{15}}{14}y_4^{-2} \tag{49}$$

$$y_2^{-2}y_2^{1}\sqrt{\pi} = -\frac{\sqrt{15}}{14}y_2^{-1} - \frac{\sqrt{70}}{28}y_4^{-3} + \frac{\sqrt{10}}{28}y_4^{-1} \tag{50}$$

$$y_2^{-2}y_2^{2}\sqrt{\pi} = \frac{\sqrt{35}}{14}y_4^{-4} \tag{51}$$

$$y_2^{-1}y_2^{-1}\sqrt{\pi} = \frac{1}{2}y_0^0 + \frac{\sqrt{5}}{14}y_2^0 - \frac{\sqrt{15}}{14}y_2^2 - \frac{2}{7}y_4^0 - \frac{\sqrt{5}}{7}y_4^2 \tag{52}$$

$$y_2^{-1}y_2^{0}\sqrt{\pi} = \frac{\sqrt{5}}{14}y_2^{-1} + \frac{\sqrt{30}}{14}y_4^{-1} \tag{53}$$

$$y_2^{-1}y_2^{1}\sqrt{\pi} = -\frac{\sqrt{15}}{14}y_2^{-2} - \frac{\sqrt{5}}{7}y_4^{-2} \tag{54}$$

$$y_2^{-1}y_2^{2}\sqrt{\pi} = -\frac{\sqrt{15}}{14}y_2^{-1} + \frac{\sqrt{70}}{28}y_4^{-3} + \frac{\sqrt{10}}{28}y_4^{-1} \tag{55}$$

$$y_2^{0}y_2^{0}\sqrt{\pi} = \frac{1}{2}y_0^0 + \frac{\sqrt{5}}{7}y_2^0 + \frac{3}{7}y_4^0 \tag{56}$$

$$y_2^{0}y_2^{1}\sqrt{\pi} = \frac{\sqrt{5}}{14}y_2^1 + \frac{\sqrt{30}}{14}y_4^1 \tag{57}$$

$$y_2^{0}y_2^{2}\sqrt{\pi} = -\frac{\sqrt{5}}{7}y_2^2 + \frac{\sqrt{15}}{14}y_4^2 \tag{58}$$

B Paraxial coherent transfer function

In this appendix we calculate the paraxial CTF for a single-view fluorescence microscope. We start by plugging Eq. 13 (the paraxial CSF) into Eq. 22

$$\mathbf{E}_l^{m(p)}(\boldsymbol{\nu}) \propto \int_{\mathbb{S}^2} d\hat{\mathbf{s}}_o \int_{\mathbb{R}^2} d\mathbf{r}'_d \begin{bmatrix} A^{(p)}(r'_d) y_1^1(\hat{\mathbf{s}}_o) + 2iB^{(p)}(r'_d)\cos\phi'_d y_1^0(\hat{\mathbf{s}}_o) \\ A^{(p)}(r'_d) y_1^{-1}(\hat{\mathbf{s}}_o) + 2iB^{(p)}(r'_d)\sin\phi'_d y_1^0(\hat{\mathbf{s}}_o) \\ 0 \end{bmatrix} y_l^m(\hat{\mathbf{s}}_o)\, \mathrm{e}^{-i2\pi \mathbf{r}'_d\cdot\boldsymbol{\nu}}. \tag{62}$$

We split the integral into two parts by writing

$$\mathbf{E}_l^{m(p)}(\boldsymbol{\nu}) \propto \int_{\mathbb{S}^2} d\hat{\mathbf{s}}_o\, \mathbf{E}^{(p)}(\boldsymbol{\nu};\hat{\mathbf{s}}_o) y_l^m(\hat{\mathbf{s}}_o), \tag{63}$$

$$\mathbf{E}^{(p)}(\boldsymbol{\nu};\hat{\mathbf{s}}_o) \equiv \int_{\mathbb{R}^2} d\mathbf{r}'_d \begin{bmatrix} A^{(p)}(r'_d) y_1^1(\hat{\mathbf{s}}_o) + 2iB^{(p)}(r'_d)\cos\phi'_d y_1^0(\hat{\mathbf{s}}_o) \\ A^{(p)}(r'_d) y_1^{-1}(\hat{\mathbf{s}}_o) + 2iB^{(p)}(r'_d)\sin\phi'_d y_1^0(\hat{\mathbf{s}}_o) \\ 0 \end{bmatrix} \mathrm{e}^{-i2\pi \mathbf{r}'_d\cdot\boldsymbol{\nu}}. \tag{64}$$

Substituting $A^{(p)}(r'_d)$ and $B^{(p)}(r'_d)$ using Eq. 14 gives

$$\mathbf{E}^{(p)}(\boldsymbol{\nu};\hat{\mathbf{s}}_o) = \int_{\mathbb{R}^2} d\mathbf{r}'_d \begin{bmatrix} \frac{J_1(2\pi a r'_d)}{\pi a r'_d} y_1^m(\hat{\mathbf{s}}_o) + 2i\frac{\mathrm{NA}}{n_o}\left[\frac{J_2(2\pi a r'_d)}{\pi a r'_d}\right]\cos\phi'_d y_1^0(\hat{\mathbf{s}}_o) \\ \frac{J_1(2\pi a r'_d)}{\pi a r'_d} y_1^{-1}(\hat{\mathbf{s}}_o) + 2i\frac{\mathrm{NA}}{n_o}\left[\frac{J_2(2\pi a r'_d)}{\pi a r'_d}\right]\sin\phi'_d y_1^0(\hat{\mathbf{s}}_o) \\ 0 \end{bmatrix} \mathrm{e}^{-i2\pi \mathbf{r}'_d\cdot\boldsymbol{\nu}}. \tag{65}$$

We can rewrite this in terms of three two-dimensional Fourier transforms

$$\mathbf{E}^{(p)}(\boldsymbol{\nu};\hat{\mathbf{s}}_o) \propto \begin{bmatrix} t_1(\boldsymbol{\nu}) y_1^1(\hat{\mathbf{s}}_o) + t_2(\boldsymbol{\nu}) y_1^0(\hat{\mathbf{s}}_o) \\ t_1(\boldsymbol{\nu}) y_1^{-1}(\hat{\mathbf{s}}_o) + t_3(\boldsymbol{\nu}) y_1^0(\hat{\mathbf{s}}_o) \\ 0 \end{bmatrix} \tag{66}$$

where

$$t_1(\boldsymbol{\nu}) \equiv \frac{1}{\pi a}\int_{\mathbb{R}^2} d\mathbf{r}'_d\, \frac{J_1(2\pi a r'_d)}{r'_d}\, \mathrm{e}^{-i2\pi \mathbf{r}'_d\cdot\boldsymbol{\nu}}, \tag{67}$$

$$t_2(\boldsymbol{\nu}) \equiv \frac{2i}{\pi a}\frac{\mathrm{NA}}{n_o}\int_{\mathbb{R}^2} d\mathbf{r}'_d\, \frac{J_2(2\pi a r'_d)}{r'_d}\cos\phi'_d\, \mathrm{e}^{-i2\pi \mathbf{r}'_d\cdot\boldsymbol{\nu}}, \tag{68}$$

$$t_3(\boldsymbol{\nu}) \equiv \frac{2i}{\pi a}\frac{\mathrm{NA}}{n_o}\int_{\mathbb{R}^2} d\mathbf{r}'_d\, \frac{J_2(2\pi a r'_d)}{r'_d}\sin\phi'_d\, \mathrm{e}^{-i2\pi \mathbf{r}'_d\cdot\boldsymbol{\nu}}. \tag{69}$$

All three of the functions to be transformed are separable in polar coordinates, so we can rewrite the Fourier transform as a sum of weighted Hankel transforms [3]. In general, if a function $g(r,\theta)$ is separable in polar coordinates then we can rewrite it as $g(r,\theta) = g_R(r)g_\Theta(\theta)$ and its two-dimensional Fourier transform is given by

$$\mathcal{F}\{g(r,\theta)\} = \sum_{k=-\infty}^{\infty} c_k(-i)^k \mathrm{e}^{ik\phi}\mathcal{H}_k\{g_R(r)\} \tag{70}$$

where

$$c_k = \frac{1}{2\pi}\int_0^{2\pi} d\theta\, g_\Theta(\theta)\mathrm{e}^{-ik\theta} \tag{71}$$

and $\mathcal{H}_k\{\}$ is the Hankel transform of order k given by

$$\mathcal{H}_k\{g_R(r)\} = 2\pi\int_0^\infty dr\, r g_R(r) J_k(2\pi r\nu). \tag{72}$$

First, we evaluate $t_1(\boldsymbol{\nu})$. The Fourier transform will be in polar coordinates, so we define polar coordinates in frequency space as $\boldsymbol{\nu} \equiv \nu\cos\phi_\nu\hat{\mathbf{x}} + \nu\sin\phi_\nu\hat{\mathbf{y}} \equiv \nu_x\hat{\mathbf{x}} + \nu_y\hat{\mathbf{y}}$. The angular part of $J_z(ar'_d)/r'_d$ is a constant, so $c_k = \delta(k)$ which means we only need to evaluate the zero-order Hankel transform

$$t_1(\boldsymbol{\nu}) = \frac{1}{\pi a}\mathcal{H}_0\left\{\frac{J_1(2\pi a r'_d)}{r'_d}\right\}. \tag{73}$$

From tabulated Hankel transforms we find that

$$\mathcal{H}_\mu\left\{\frac{J_{\mu+1}(2\pi a r'_d)}{r'_d}\right\} = \frac{1}{2\pi}a^{-\mu-1}\nu^\mu\,\Pi\left(\frac{\nu}{a}\right) \tag{74}$$

when $a > 0$ and $\mathrm{Re}(\mu) > -\frac{3}{2}$ [6]. Applying this result we find that

$$t_1(\boldsymbol{\nu}) = \frac{1}{2\pi^2 a^2}\,\Pi\left(\frac{\nu}{a}\right). \tag{75}$$

To evaluate $t_2(\boldsymbol{\nu})$ and $t_3(\boldsymbol{\nu})$ we need to be careful with the angular part. For $t_2(\boldsymbol{\nu})$ the angular part of the function is $\cos\phi'_d = \frac{1}{2}\left(e^{i\phi'_d} + e^{-i\phi'_d}\right)$. Therefore, $c_k = \frac{1}{2}\delta(k-1) + \frac{1}{2}\delta(k+1)$ and we have to evaluate two Hankel transforms given by

$$t_2(\boldsymbol{\nu}) = \frac{2i}{\pi a}\frac{\mathrm{NA}}{n_o}\left[ie^{-i\phi_\nu}\mathcal{H}_{-1}\left\{\frac{J_2(2\pi a r'_d)}{\pi a r'_d}\right\} - ie^{i\phi_\nu}\mathcal{H}_1\left\{\frac{J_2(2\pi a r'_d)}{\pi a r'_d}\right\}\right]. \tag{76}$$

To put the Hankel transforms in the form of Eq. 74 we apply $\mathcal{H}_\mu = (-1)^\mu\mathcal{H}_{-\mu}$ to get

$$t_2(\boldsymbol{\nu}) = \frac{2i}{\pi a}\frac{\mathrm{NA}}{n_o}\left[-ie^{-i\phi_\nu}\mathcal{H}_1\left\{\frac{J_2(2\pi a r'_d)}{\pi a r'_d}\right\} - ie^{i\phi_\nu}\mathcal{H}_1\left\{\frac{J_2(2\pi a r'_d)}{\pi a r'_d}\right\}\right]. \tag{77}$$

Applying Eq. 74 and simplifying gives

$$t_2(\boldsymbol{\nu}) = \frac{1}{\pi^2 a^3}\frac{\mathrm{NA}}{n_o}\nu(e^{-i\phi_\nu} + e^{i\phi_\nu})\,\Pi\left(\frac{\nu}{a}\right) \tag{78}$$

Finally,

$$t_2(\boldsymbol{\nu}) = \frac{1}{\pi^2 a^3}\frac{\mathrm{NA}}{n_o}\nu\cos\phi_\nu\,\Pi\left(\frac{\nu}{a}\right) \tag{79}$$

Similarly,

$$t_3(\boldsymbol{\nu}) = \frac{1}{\pi^2 a^3}\frac{\mathrm{NA}}{n_o}\nu\sin\phi_\nu\,\Pi\left(\frac{\nu}{a}\right) \tag{80}$$

Plugging Eqs. 75, 79, and 80 into Eq. 66 and normalizing gives

$$\mathbf{E}^{(p)}(\boldsymbol{\nu};\hat{\mathbf{s}}_o) = \begin{bmatrix} y_1^1(\hat{\mathbf{s}}_o) + \frac{2}{a}\frac{\mathrm{NA}}{n_o}\nu\cos\phi_\nu y_1^0(\hat{\mathbf{s}}_o) \\ y_1^{-1}(\hat{\mathbf{s}}_o) + \frac{2}{a}\frac{\mathrm{NA}}{n_o}\nu\sin\phi_\nu y_1^0(\hat{\mathbf{s}}_o) \\ 0 \end{bmatrix}\,\Pi\left(\frac{\nu}{a}\right). \tag{81}$$

Finally, we find the paraxial CTF by evaluating the angular integral in Eq. 64

$$\mathbf{E}_l^{m(p)}(\boldsymbol{\nu}) = \begin{bmatrix} \delta(l-1,m-1) + \frac{2}{a}\frac{\mathrm{NA}}{n_o}\nu\cos\phi_\nu\delta(l-1,m) \\ \delta(l-1,m+1) + \frac{2}{a}\frac{\mathrm{NA}}{n_o}\nu\sin\phi_\nu\delta(l-1,m) \\ 0 \end{bmatrix}\,\Pi\left(\frac{\nu}{a}\right). \tag{82}$$

C Paraxial optical transfer function

In this appendix we calculate the paraxial OTF for a single-view fluorescence microscope. We start with Eq. 83

$$H_l^m(\boldsymbol{\nu}) \propto \int_{\mathbb{S}^2} d\hat{\mathbf{s}}_o \int_{\mathbb{R}^2} d\mathbf{r}'_d \, h(\mathbf{r}'_d, \hat{\mathbf{s}}_o) y_l^m(\hat{\mathbf{s}}_o) \, \mathrm{e}^{-i2\pi \mathbf{r}'_d \cdot \boldsymbol{\nu}}. \tag{83}$$

We could plug in the paraxial PSF and evaluate the integrals, but this will lead us to Fourier transforms that cannot be found in tables. Instead we use a trick from scalar Fourier optics and write the OTF in terms of the detected electric field [3]

$$H_l^m(\boldsymbol{\nu}) \propto \int_{\mathbb{S}^2} d\hat{\mathbf{s}}_o \int_{\mathbb{R}^2} d\mathbf{r}'_d \, \left|\mathbf{e}_d(\mathbf{r}'_d, \hat{\mathbf{s}}_o)\right|^2 y_l^m(\hat{\mathbf{s}}_o) \, \mathrm{e}^{-i2\pi \mathbf{r}'_d \cdot \boldsymbol{\nu}}. \tag{84}$$

Next, we manipulate this equation to

$$H_l^m(\boldsymbol{\nu}) \propto \int_{\mathbb{S}^2} d\hat{\mathbf{s}}_o \, y_l^m(\hat{\mathbf{s}}_o) \int_{\mathbb{R}^2} d\mathbf{r}'_d \, \mathbf{e}_d^\dagger(\mathbf{r}'_d, \hat{\mathbf{s}}_o) \mathbf{e}_d(\mathbf{r}'_d, \hat{\mathbf{s}}_o) \, \mathrm{e}^{-i2\pi \mathbf{r}'_d \cdot \boldsymbol{\nu}}, \tag{85}$$

$$H_l^m(\boldsymbol{\nu}) \propto \int_{\mathbb{S}^2} d\hat{\mathbf{s}}_o \, y_l^m(\hat{\mathbf{s}}_o) \int_{\mathbb{R}^2} d\mathbf{r}'_d \int_{\mathbb{R}^2} d\mathbf{r}''_d \, \mathbf{e}_d^\dagger(\mathbf{r}'_d, \hat{\mathbf{s}}_o) \mathbf{e}_d(\mathbf{r}''_d, \hat{\mathbf{s}}_o) \delta(\mathbf{r}''_d - \mathbf{r}'_d) \, \mathrm{e}^{-i2\pi \mathbf{r}''_d \cdot \boldsymbol{\nu}}, \tag{86}$$

$$H_l^m(\boldsymbol{\nu}) \propto \int_{\mathbb{S}^2} d\hat{\mathbf{s}}_o \, y_l^m(\hat{\mathbf{s}}_o) \int_{\mathbb{R}^2} d\boldsymbol{\tau} \int_{\mathbb{R}^2} d\mathbf{r}'_d \int_{\mathbb{R}^2} d\mathbf{r}''_d \, \mathbf{e}_d^\dagger(\mathbf{r}'_d, \hat{\mathbf{s}}_o) \mathbf{e}_d(\mathbf{r}''_d, \hat{\mathbf{s}}_o) \mathrm{e}^{-i2\pi \boldsymbol{\tau} (\mathbf{r}''_d - \mathbf{r}'_d)} \mathrm{e}^{-i2\pi \mathbf{r}''_d \cdot \boldsymbol{\nu}}, \tag{87}$$

$$H_l^m(\boldsymbol{\nu}) \propto \int_{\mathbb{S}^2} d\hat{\mathbf{s}}_o \, y_l^m(\hat{\mathbf{s}}_o) \int_{\mathbb{R}^2} d\boldsymbol{\tau} \left[\int_{\mathbb{R}^2} d\mathbf{r}'_d \, \mathbf{e}_d^\dagger(\mathbf{r}'_d, \hat{\mathbf{s}}_o) \mathrm{e}^{i2\pi \mathbf{r}'_d \cdot \boldsymbol{\nu}}\right] \left[\int_{\mathbb{R}^2} d\mathbf{r}''_d \, \mathbf{e}_d(\mathbf{r}''_d, \hat{\mathbf{s}}_o) \mathrm{e}^{-i2\pi \mathbf{r}''_d \cdot (\boldsymbol{\nu} + \boldsymbol{\tau})}\right], \tag{88}$$

$$H_l^m(\boldsymbol{\nu}) \propto \int_{\mathbb{S}^2} d\hat{\mathbf{s}}_o \, y_l^m(\hat{\mathbf{s}}_o) \int_{\mathbb{R}^2} d\boldsymbol{\tau} \, \mathbf{E}^\dagger(\boldsymbol{\tau}; \hat{\mathbf{s}}_o) \mathbf{E}(\boldsymbol{\tau} + \boldsymbol{\nu}; \hat{\mathbf{s}}_o). \tag{89}$$

We have followed the proof for the Wiener-Kinchin theorem [4, 7] to explicitly show how the angular integral affects the usual scalar calculation. Eq. 89 shows that we can calculate the OTF by taking the vector autocorrelation of the spatial CTF then projecting the result onto the spherical harmonics.

We will rewrite Eq. 89 in two parts

$$H_l^m(\boldsymbol{\nu}) \propto \int_{\mathbb{S}^2} d\hat{\mathbf{s}}_o \, y_l^m(\hat{\mathbf{s}}_o) H(\boldsymbol{\nu}; \hat{\mathbf{s}}_o) \tag{90}$$

$$H(\boldsymbol{\nu}; \hat{\mathbf{s}}_o) \equiv \int_{\mathbb{R}^2} d\boldsymbol{\tau} \, \mathbf{E}^\dagger(\boldsymbol{\tau} - \boldsymbol{\nu}/2; \hat{\mathbf{s}}_o) \mathbf{E}(\boldsymbol{\tau} + \boldsymbol{\nu}/2; \hat{\mathbf{s}}_o). \tag{91}$$

Notice the change of variable to simplify the autocorrelation. In the previous section we calculated the CTF in the paraxial case as

$$\mathbf{E}^{(p)}(\boldsymbol{\nu}; \hat{\mathbf{s}}_o) = \begin{bmatrix} y_1^1(\hat{\mathbf{s}}_o) + \frac{2}{a}\frac{\mathrm{NA}}{n_o} \nu \cos\phi_\nu y_1^0(\hat{\mathbf{s}}_o) \\ y_1^{-1}(\hat{\mathbf{s}}_o) + \frac{2}{a}\frac{\mathrm{NA}}{n_o} \nu \sin\phi_\nu y_1^0(\hat{\mathbf{s}}_o) \\ 0 \end{bmatrix} \Pi\left(\frac{\nu}{a}\right). \tag{92}$$

By introducing $\boldsymbol{\tau} \equiv \tau_x \hat{\mathbf{x}} + \tau_y \hat{\mathbf{y}} \equiv \tau \cos\phi_\tau \hat{\mathbf{x}} + \tau \sin\phi_\tau \hat{\mathbf{y}}$ we can plug Eq. 92 into Eq. 91 and find that

$$H^{(p)}(\boldsymbol{\nu}; \hat{\mathbf{s}}_o) = \int_{\mathbb{R}^2} d\boldsymbol{\tau} \begin{bmatrix} y_1^1(\hat{\mathbf{s}}_o) + \frac{2}{a}\frac{\mathrm{NA}}{n_o}(\tau_x - \frac{1}{2}\nu_x) y_1^0(\hat{\mathbf{s}}_o) \\ y_1^{-1}(\hat{\mathbf{s}}_o) + \frac{2}{a}\frac{\mathrm{NA}}{n_o}(\tau_y - \frac{1}{2}\nu_y) y_1^0(\hat{\mathbf{s}}_o) \\ 0 \end{bmatrix}^\dagger \begin{bmatrix} y_1^1(\hat{\mathbf{s}}_o) + \frac{2}{a}\frac{\mathrm{NA}}{n_o}(\tau_x + \frac{1}{2}\nu_x) y_1^0(\hat{\mathbf{s}}_o) \\ y_1^{-1}(\hat{\mathbf{s}}_o) + \frac{2}{a}\frac{\mathrm{NA}}{n_o}(\tau_y + \frac{1}{2}\nu_y) y_1^0(\hat{\mathbf{s}}_o) \\ 0 \end{bmatrix} \Pi\left(\frac{\tau - \nu/2}{a}\right) \Pi\left(\frac{\tau + \nu/2}{a}\right). \tag{93}$$

Expanding the inner product gives

$$H^{(p)}(\boldsymbol{\nu};\hat{\mathbf{s}}_o) = \int_{\mathbb{R}^2} d\boldsymbol{\tau}\, \{y_1^1(\hat{\mathbf{s}}_o)\}^2 + \left\{\frac{2}{a}\frac{\mathrm{NA}}{n_o} y_1^0(\hat{\mathbf{s}}_o)\right\}^2 (\tau_x - \frac{1}{2}\nu_x)(\tau_x + \frac{1}{2}\nu_x) + \{y_1^{-1}(\hat{\mathbf{s}}_o)\}^2 + \left\{\frac{2}{a}\frac{\mathrm{NA}}{n_o} y_1^0(\hat{\mathbf{s}}_o)\right\}^2 (\tau_y - \frac{1}{2}\nu_y)(\tau_y + \frac{1}{2}\nu_y) + \left\{\frac{2}{a}\frac{\mathrm{NA}}{n_o} y_1^0(\hat{\mathbf{s}}_o) y_1^1(\hat{\mathbf{s}}_o)\right\}(\tau_x - \frac{1}{2}\nu_x) + \left\{\frac{2}{a}\frac{\mathrm{NA}}{n_o} y_1^0(\hat{\mathbf{s}}_o) y_1^1(\hat{\mathbf{s}}_o)\right\}(\tau_x + \frac{1}{2}\nu_x) \left\{\frac{2}{a}\frac{\mathrm{NA}}{n_o} y_1^0(\hat{\mathbf{s}}_o) y_1^{-1}(\hat{\mathbf{s}}_o)\right\}(\tau_y - \frac{1}{2}\nu_y) + \left\{\frac{2}{a}\frac{\mathrm{NA}}{n_o} y_1^0(\hat{\mathbf{s}}_o) y_1^{-1}(\hat{\mathbf{s}}_o)\right\}(\tau_y + \frac{1}{2}\nu_y) \Pi\left(\frac{\tau - \nu/2}{a}\right)\Pi\left(\frac{\tau + \nu/2}{a}\right). \tag{94}$$

All of the terms with a single τ_x or τ_y are odd, so they integrate to zero. Therefore

$$H^{(p)}(\boldsymbol{\nu};\hat{\mathbf{s}}_o) = \int_{\mathbb{R}^2} d\boldsymbol{\tau}\, \{y_1^1(\hat{\mathbf{s}}_o)\}^2 + \left\{\frac{2}{a}\frac{\mathrm{NA}}{n_o} y_1^0(\hat{\mathbf{s}}_o)\right\}^2 (\tau_x - \frac{1}{2}\nu_x)(\tau_x + \frac{1}{2}\nu_x) + \{y_1^{-1}(\hat{\mathbf{s}}_o)\}^2 + \left\{\frac{2}{a}\frac{\mathrm{NA}}{n_o} y_1^0(\hat{\mathbf{s}}_o)\right\}^2 (\tau_y - \frac{1}{2}\nu_y)(\tau_y + \frac{1}{2}\nu_y) + \Pi\left(\frac{\tau - \nu/2}{a}\right)\Pi\left(\frac{\tau + \nu/2}{a}\right). \tag{95}$$

After expanding the spherical harmonics we can rewrite this equation in terms of three autocorrelations

$$H^{(p)}(\boldsymbol{\nu};\hat{\mathbf{s}}_o) = [s_1(\boldsymbol{\nu}) + s_2(\boldsymbol{\nu}) + s_3(\boldsymbol{\nu})] y_0^0(\hat{\mathbf{s}}_o) + \frac{2\mathrm{NA}}{\sqrt{5} a n_o}[-s_1(\boldsymbol{\nu}) + s_2(\boldsymbol{\nu}) + s_3(\boldsymbol{\nu})] y_2^0(\hat{\mathbf{s}}_o) \tag{96}$$

where

$$s_1(\boldsymbol{\nu}) \equiv \int_{\mathbb{R}^2} d\boldsymbol{\tau}\, \Pi\left(\frac{\tau - \nu/2}{a}\right)\Pi\left(\frac{\tau + \nu/2}{a}\right), \tag{97}$$

$$s_2(\boldsymbol{\nu}) \equiv \int_{\mathbb{R}^2} d\boldsymbol{\tau}\, (\tau_x - \nu_x/2)(\tau_x + \nu_x/2)\Pi\left(\frac{\tau - \nu/2}{a}\right)\Pi\left(\frac{\tau + \nu/2}{a}\right), \tag{98}$$

$$s_3(\boldsymbol{\nu}) \equiv \int_{\mathbb{R}^2} d\boldsymbol{\tau}\, (\tau_y - \nu_y/2)(\tau_y + \nu_y/2)\Pi\left(\frac{\tau - \nu/2}{a}\right)\Pi\left(\frac{\tau + \nu/2}{a}\right). \tag{99}$$

We can evaluate these integrals with the help of the geometric construction shown in Figure 4 [3].

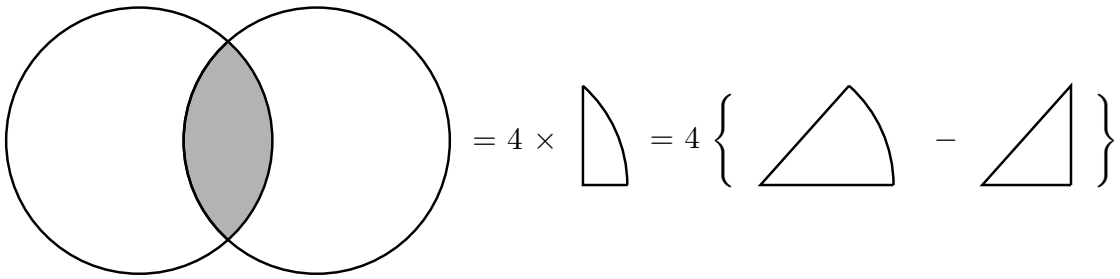

Figure 4: Geometric construction for evaluating $s_1(\boldsymbol{\nu})$, $s_2(\boldsymbol{\nu})$, and $s_3(\boldsymbol{\nu})$. We need to find the boundaries of integration for the overlapping region of two circles with radius a and distance ν between their centers. The region is given by four times the difference in area between a sector of angle $\arccos\left(\frac{\nu}{2a}\right)$ and a triangle with base $\nu/2$ and hypotenuse a.

Starting with $s_1(\boldsymbol{\nu})$ we find that

$$s_1(\boldsymbol{\nu}) = 4\left[\left(\int_0^a d\tau\,\tau \int_0^{\arccos\left(\frac{\nu}{2a}\right)} d\phi_\tau\right) - \left(\int_0^{\nu/2} d\tau_x \int_0^{\tau_x \frac{2a}{\nu}\sqrt{1-\left(\frac{\nu}{2a}\right)^2}} d\tau_y\right)\right] \tag{100}$$

$$s_1(\boldsymbol{\nu}) = 4\left[\left(\int_0^a d\tau\,\tau \arccos\left(\frac{\nu}{2a}\right)\right) - \left(\int_0^{\nu/2} d\tau_x \tau_x \frac{2a}{\nu}\sqrt{1-\left(\frac{\nu}{2a}\right)^2}\right)\right] \tag{101}$$

$$s_1(\boldsymbol{\nu}) = 4\left[\frac{a^2}{2}\arccos\left(\frac{\nu}{2a}\right) - \frac{\nu a}{4}\sqrt{1-\left(\frac{\nu}{2a}\right)^2}\right] \tag{102}$$

$$s_1(\boldsymbol{\nu}) = 2a^2\arccos\left(\frac{\nu}{2a}\right) - \nu a\sqrt{1-\left(\frac{\nu}{2a}\right)^2}. \tag{103}$$

Note that $s_1(\boldsymbol{\nu})$ is the unnormalized OTF for a single-view fluorescence microscope under the scalar approximation. Next we evaluate $s_2(\boldsymbol{\nu})$ using the same geometric construction. This integral is not rotationally symmetric, so we start by restricting $\boldsymbol{\nu}$ to the x-axis

$$\begin{aligned} s_2(\nu_x) = 4\Bigg[&\int_0^a d\tau\,\tau \int_0^{\arccos\left(\frac{\nu_x}{2a}\right)} d\phi_\tau (\tau\cos\phi_\tau - \nu_x/2)(\tau\cos\phi_\tau + \nu_x/2) \\ &- \int_0^{\nu_x/2} d\tau_x \int_0^{\tau_x \frac{2a}{\nu_x}\sqrt{1-\left(\frac{\nu_x}{2a}\right)^2}} d\tau_y (\tau_x - \nu_x/2)(\tau_x + \nu_x/2)\Bigg], \end{aligned} \tag{104}$$

$$\begin{aligned} s_2(\nu_x) = 4\Bigg[&\int_0^a d\tau\,\tau \int_0^{\arccos\left(\frac{\nu_x}{2a}\right)} d\phi_\tau (\tau^2\cos^2\phi_\tau - \nu_x^2/4) \\ &- \int_0^{\nu_x/2} d\tau_x \int_0^{\tau_x \frac{2a}{\nu_x}\sqrt{1-\left(\frac{\nu_x}{2a}\right)^2}} d\tau_y (\tau_x^2 - \nu_x^2/4)\Bigg]. \end{aligned} \tag{105}$$

For the first inner integral we will make use of the following

$$\int_0^{\arccos(z)} d\phi\cos^2\phi = \frac{1}{2}z\sqrt{1-z^2} + \frac{1}{2}\arccos(z). \tag{106}$$

This results in

$$s_2(\nu_x) = 4\Bigg[\int_0^a d\tau \left(\frac{\tau^3}{2}\left(\frac{\nu_x}{2a}\right)\sqrt{1-\left(\frac{\nu_x}{2a}\right)^2} + \frac{\tau^3}{2}\arccos\left(\frac{\nu_x}{2a}\right) - \frac{\tau\nu_x^2}{4}\arccos\left(\frac{\nu_x}{2a}\right)\right) - \int_0^{\nu_x/2} d\tau_x \left(\tau_x^3 - \frac{\tau_x\nu_x^2}{4}\right)\frac{2a}{\nu_x}\sqrt{1-\left(\frac{\nu_x}{2a}\right)^2}\Bigg], \tag{107}$$

$$s_2(\nu_x) = 4\left[\left(\frac{a^4}{8}\left(\frac{\nu_x}{2a}\right)\sqrt{1-\left(\frac{\nu_x}{2a}\right)^2} + \frac{a^4}{8}\arccos\left(\frac{\nu_x}{2a}\right) - \frac{a^2\nu_x^2}{8}\arccos\left(\frac{\nu_x}{2a}\right)\right) - \left(\frac{\nu_x^4}{64} - \frac{\nu_x^4}{32}\right)\frac{2a}{\nu_x}\sqrt{1-\left(\frac{\nu_x}{2a}\right)^2}\right], \tag{108}$$

$$s_2(\nu_x) = 4\left[\frac{\nu_x a^3}{16}\sqrt{1-\left(\frac{\nu_x}{2a}\right)^2} + \frac{a^4}{8}\arccos\left(\frac{\nu_x}{2a}\right) - \frac{a^2\nu_x^2}{8}\arccos\left(\frac{\nu_x}{2a}\right) + \frac{\nu_x^3 a}{32}\sqrt{1-\left(\frac{\nu_x}{2a}\right)^2}\right], \tag{109}$$

$$s_2(\nu_x) = \frac{\nu_x a^3}{4}\sqrt{1-\left(\frac{\nu_x}{2a}\right)^2} + \frac{a^4}{2}\arccos\left(\frac{\nu_x}{2a}\right) - \frac{a^2\nu_x^2}{2}\arccos\left(\frac{\nu_x}{2a}\right) + \frac{\nu_x^3 a}{8}\sqrt{1-\left(\frac{\nu_x}{2a}\right)^2}, \tag{110}$$

$$s_2(\nu_x) = \left(\frac{a^2}{4} - \frac{\nu_x^2}{4}\right)2a^2\arccos\left(\frac{\nu_x}{2a}\right) + \left(\frac{a^2}{4} + \frac{\nu_x^2}{8}\right)\nu_x a\sqrt{1-\left(\frac{\nu_x}{2a}\right)^2}. \tag{111}$$

This result is only true for $\boldsymbol{\nu}$ restricted to the x axis, but we can extend this result to the general case by noticing that the value of the function in the area of overlap has the same functional form for any direction of $\boldsymbol{\nu}$ but the total value is reduced by a factor of $\cos^2\phi_\nu$. This make sense because the function in the area of overlap for the circles displaced along the y-axis is zero. Therefore, the complete integral is given by

$$s_2(\boldsymbol{\nu}) = \cos^2\phi_\nu\left[\left(\frac{a^2}{4} - \frac{\nu^2}{4}\right)2a^2\arccos\left(\frac{\nu}{2a}\right) + \left(\frac{a^2}{4} + \frac{\nu^2}{8}\right)\nu a\sqrt{1-\left(\frac{\nu}{2a}\right)^2}\right]. \tag{112}$$

Similarly, $s_3(\boldsymbol{\nu})$ is given by

$$s_3(\boldsymbol{\nu}) = \sin^2\phi_\nu\left[\left(\frac{a^2}{4} - \frac{\nu^2}{4}\right)2a^2\arccos\left(\frac{\nu}{2a}\right) + \left(\frac{a^2}{4} + \frac{\nu^2}{8}\right)\nu a\sqrt{1-\left(\frac{\nu}{2a}\right)^2}\right]. \tag{113}$$

Plugging these results into Eq. 96 gives

$$H^{(p)}(\boldsymbol{\nu};\hat{\mathbf{s}}_o) = \left[\left(1 + \frac{a^2}{4} - \frac{\nu^2}{4}\right)2a^2\arccos\left(\frac{\nu}{2a}\right) - \left(1 - \frac{a^2}{4} - \frac{\nu^2}{8}\right)\nu a\sqrt{1-\left(\frac{\nu}{2a}\right)^2}\right]y_0^0(\hat{\mathbf{s}}_o) + \left[\left(-1 + \frac{a^2}{4} - \frac{\nu^2}{4}\right)2a^2\arccos\left(\frac{\nu}{2a}\right) - \left(-1 - \frac{a^2}{4} - \frac{\nu^2}{8}\right)\nu a\sqrt{1-\left(\frac{\nu}{2a}\right)^2}\right]y_2^0(\hat{\mathbf{s}}_o). \tag{114}$$

After plugging this into Eq. 90, performing the angular integral, refactoring, and normalizing, we get the complete spatio-angular transfer function

$$H_l^m(\nu) = H_0^0(\nu)\delta(l,m) + \frac{2\mathrm{NA}}{\sqrt{5}an_o}H_2^0(\nu)\delta(l-2,m) \tag{115}$$

$$H_0^0(\nu) = \left(1 + \frac{a^2}{4} - \frac{\nu^2}{4}\right)2a^2\arccos\left(\frac{\nu}{2a}\right) - \left(1 - \frac{a^2}{4} - \frac{\nu^2}{8}\right)\nu a\sqrt{1-\left(\frac{\nu}{2a}\right)^2} \tag{116}$$

$$H_2^0(\nu) = \left(-1 + \frac{a^2}{4} - \frac{\nu^2}{4}\right)2a^2\arccos\left(\frac{\nu}{2a}\right) - \left(-1 - \frac{a^2}{4} - \frac{\nu^2}{8}\right)\nu a\sqrt{1-\left(\frac{\nu}{2a}\right)^2} \tag{117}$$